Active Cloud Probing with Los Alamos National Laboratory's Wide Angle Imaging Lidar: Status and Outlook

I.N. Polonsky, A.B. Davis, S.P. Love, and S.P. Brumby
Los Alamos National Laboratory
Los Alamos, New Mexico

Summary

We survey recent developments in off-beam cloud lidar and especially the Wide Angle Imaging Lidar (WAIL) developed at Los Alamos National Laboratory (LANL). By abandoning the single back-scattering assumption of standard (on-beam) lidar in favor of a multiple scattering model and with the appropriate modifications of the instrument, we enable detection robust detection of the cloud boundary opposite to the source, hence cloud thickness (as well as altitude). We can also determine a volume-averaged extinction at 532 nm, hence mean cloud optical depth. Comparisons with Atmospheric Radiation Measurement (ARM) program instruments targeting the same cloud properties are already good and easily improvable. Finally, we describe several extensions of WAIL capability at various stages of planning and realization.

Off-Beam Cloud Lidar Concept and Designs

The principle of off-beam lidar operation is predicated on the fact that multiply-scattered light starting and ending at a cloud boundary thoroughly samples the interior of a dense non-absorbing medium (Davis et al. 1997). So, if an optically thick cloud is targeted, the characteristics of the reflected radiance distribution in space, angle and time will depend on its optical and geometrical properties. Photons should be collected within a receiver field of view (FOV) wide enough to take in essentially the entire spatial distribution of the reflected radiance at the medium boundary, and this should enable the retrieval of both geometrical thickness H and a volume-averaged extinction coefficient σ (equivalently, the mean optical depth $\tau = \sigma H$).

Off-beam lidar competes with millimeter wave radar as a probe of cloud structure in the sense of height, thickness and, to some extent, density. It will of course not yield the same spatial detail as mm-radar since our lidar-based estimates of H and τ are inherently averaged horizontally, nor is detailed stratification information available at present. In millimeter wave radars, reflectivity is however weighted towards the largest droplets. It therefore responds very strongly to drizzle. So much in fact

that retrievals of interest in climate studies can be compromised if any precipitation is present (Clothiaux et al. 1995). We view off-beam lidar as a natural extension of standard (on-beam) lidar and as a complement to mm-radar at a visible wavelength that bears directly on the climatic impact of clouds in the solar spectrum.

At present there are two off-beam lidar systems in existence for remote observation. The THickness from Offbeam Returns (THOR) system (Cahalan et al. 2005), developed at National Aeronautic and Space Administration (NASA) Goddard Space Flight Center, is operated from an aircraft in downward-looking configuration from well above cloud top. The upward-looking WAIL system (Polonsky et al. 2005) was designed at LANL for ground-based observations. A third system, the "in situ" cloud lidar (Evans et al. 2003) is under development as a payload for aircraft flying inside the clouds. The current prototype was constructed as part of a NASA-Goddard/University of Colorado/Spec, Inc. Small Business Innovation Research (grant) project. It is presently in the advanced testing stage.

The major difference between THOR and WAIL is their receivers. WAIL is a fully imaging implementation of the off-beam lidar concept and its gated/intensified charge-coupled device (CCD) imager uses a 256×256 pixel array (reduced to 128×128 in the present analysis) resulting in a square FOV at the focal plane, 53.6° on a side (roughly $0.42° \times 0.42°$ per pixel). WAIL's receiver also has the unique capability of varying the size of its time bins during the data acquisition; this feature is convenient for managing the signal-to-noise ratio which varies considerably across the space+time data-cube. THOR's receiver consists of a central narrow FOV and seven concentric annular rings, all manifested at the focal plane by fiber-optic bundles. The outermost ring is equally divided among three parts, that each see one of three 120° azimuthal sectors. The total FOV of THOR is roughly 6.1°. This ten-fold difference is because THOR is an airborne device assumed to be 10 or so km above the cloud deck while WAIL is designed to operate from below the cloud deck.

The in-cloud active cloud probe described by Evans et al. makes no atemp at partitioning the incoming scattered photons by angle; it operates only in the time domain. This strategy has already been successfully used by Davis et al. (2001) to analyze lidar return signals from a dense marine stratocumulus deck captured during the Lidar In space Technology Experiment (Winker et al. 1996) which was flown in September 1994 on the Discovery Space Shuttle mission (STS-64). Indeed, a relatively standard lidar receiver FOV of 3.5 mrad at an orbital range of 260 km subtends a circular footprint of 910 m in diameter, very large by lidar standards. This scale is several times the characteristic distance of horizontal photon transport by multiple scattering in such clouds, namely, 200-300 m (Marshak et al. 1995). So essentially all orders of scattering are present in the detected signal.

Deployment at the ARM Southern Great Plains (SGP) Site on 25 March 2002

During the night of March 24-25, 2002, WAIL was deployed at the Lamont, Oklahoma, ARM Climate Research Facility (ACRF) alongside the cloud-probing systems operating routinely (see Figure 1): a microwave radiometer, a millimeter wave cloud radar, a Vaisala ceilometer, and a micro-pulse lidar (MPL), while THOR was looking down from NASA's P-3 aircraft (and used here as an independent cloud-top detector). This suite of instruments was used to probe an extensive cloud layer above the site, thus enabling a direct comparison of the WAIL with more conventional instruments.

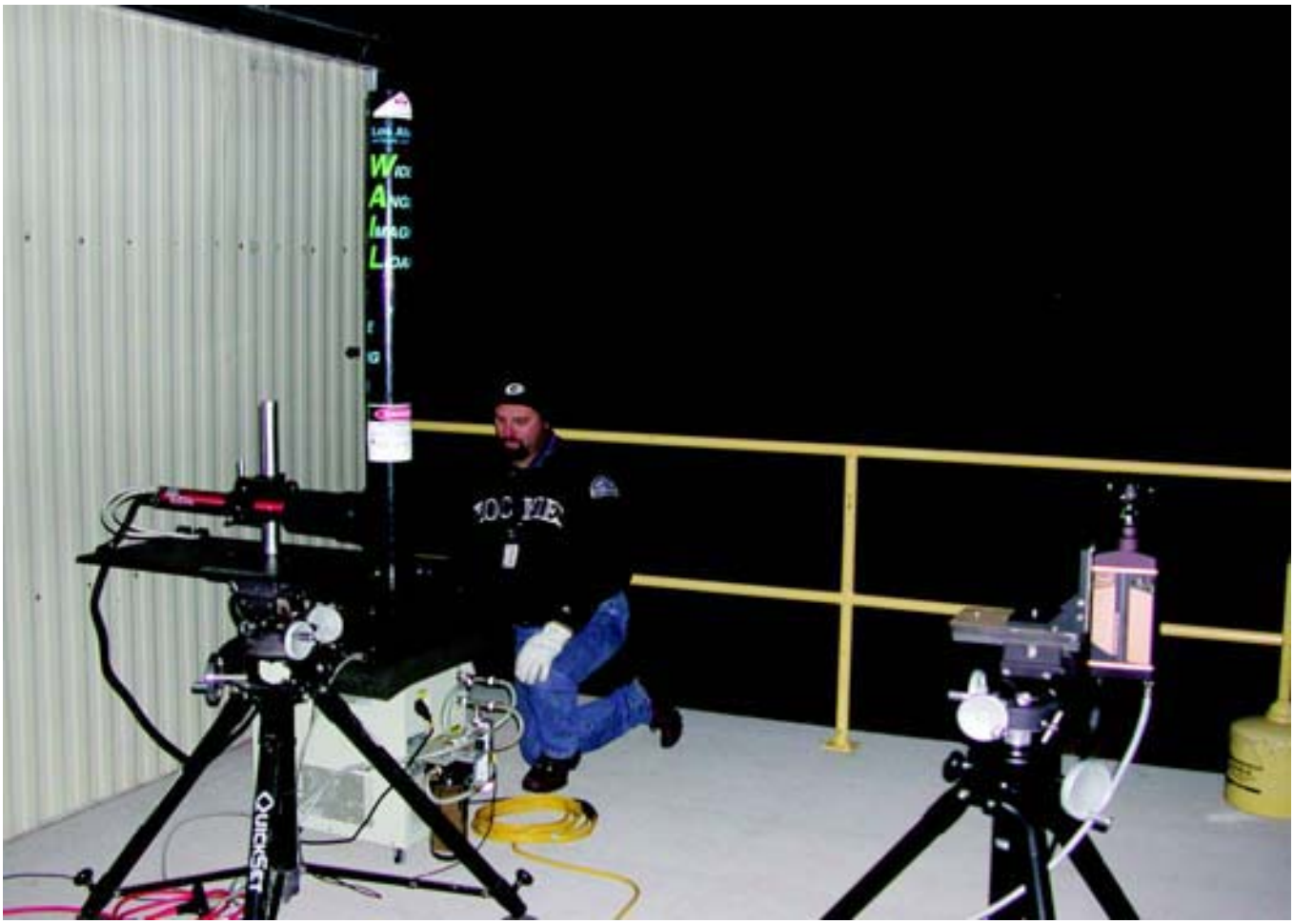

Figure 1. WAIL deployed on the guest-instrument platform at the ARM SGP site near Lamont, Oklahoma, in March 2002. To the left, LANL technician Larry Tellier is attending the water-cooled laser transmitter, a doubled Nd:YAG (532 nm); a typical rep rate was 4 kHz for a pulse energy of 0.5 mJ. The gated/intensified CCD receiver is to the right. The data acquisition computer is not in view. All these components are commercially available.

Davis et al. (1999) originally proposed to exploit their analytical expressions for the spatial and temporal moments of the radiative transfer Green function (exited by the pulsed laser) which were based on the diffusion approximation, with the assumption of cloud homogeneity. However, to be useful in retrieval mode these results assume that all the significant orders-of-scattering (typically up to 100s) are captured by the detector.

To analyze the WAIL data in Figure 2, which are spatially truncated, a new theory was developed that yields an explicit expression for the Green function observed by WAIL or THOR (Polonsky and Davis 2004). To obtain the key cloud parameters, geometrical thickness and mean extinction coefficient,

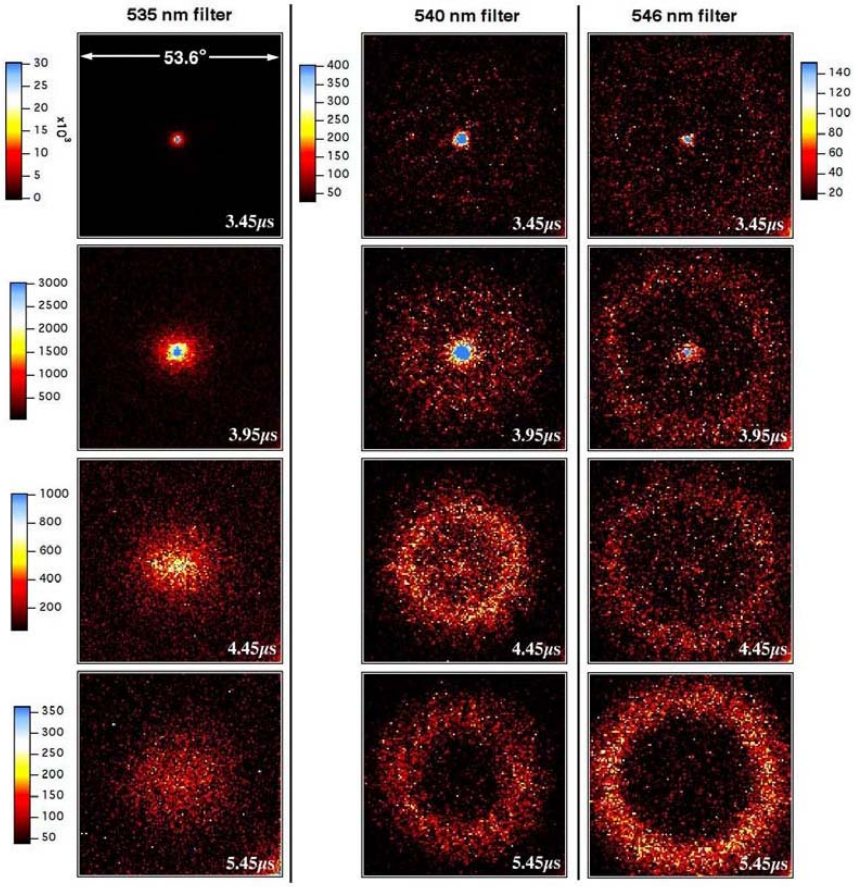

we

Figure 2. Typical frames from WAIL "movies." These datacubes are spatial/directional and temporal samples of the remotely observable (boundary) Green function of the cloud under observation for the three dimensional radiative transfer equation. Each frame has a 53.6° square FOV. In each sequence, one sees the initial impact of the laser pulse on the cloud, with subsequent decay and diffusive spreading of the light via multiple scattering. From left to right we see sampled time-bins of the raw WAIL output for three background suppression filters (535 ± 5 nm, 540 ± 5 nm, 546 ± 5 nm), each with its specific angular band pass shown in Figure 3. Notice the dramatic change of scale between the different frames.

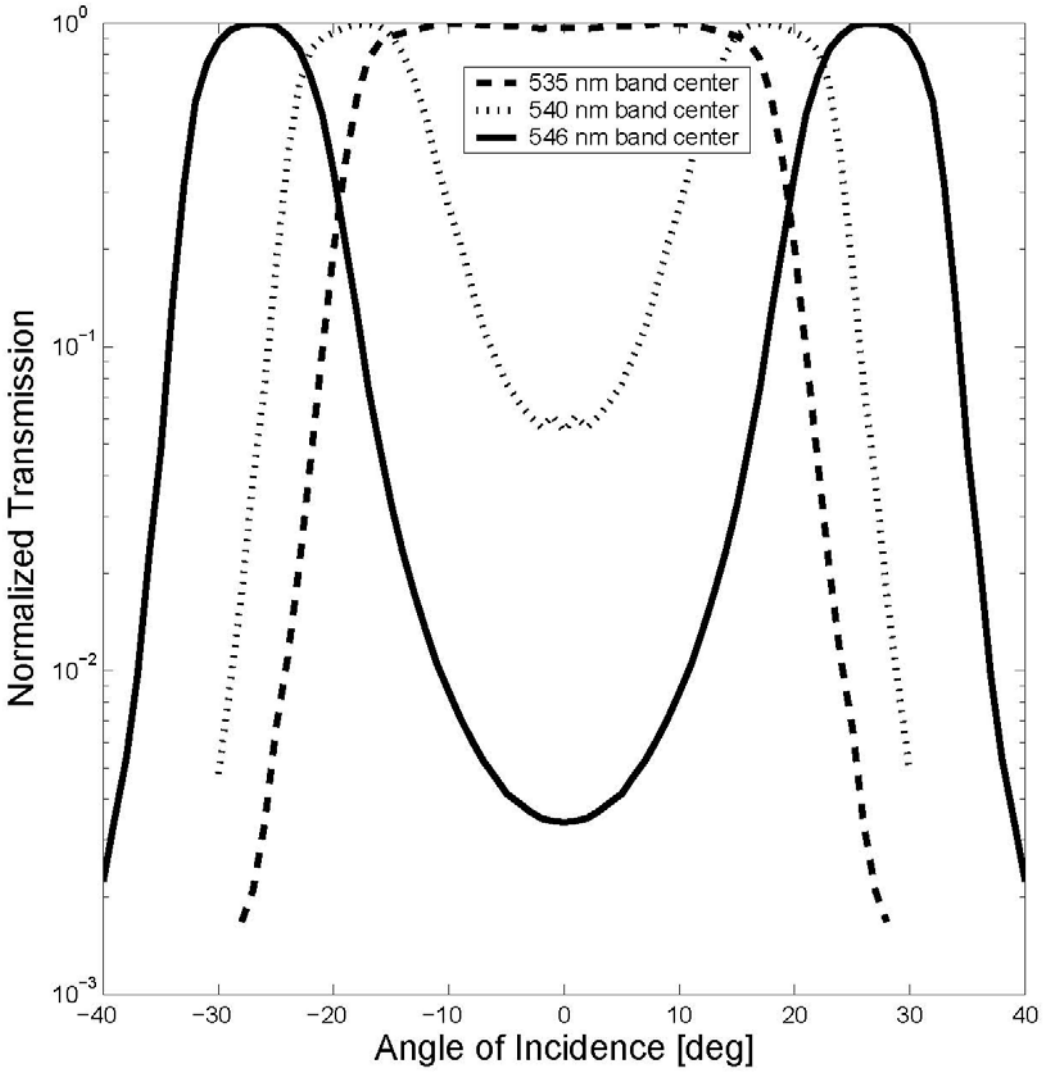

Figure 3. The angular response of the interference filters used in the current WAIL receiver, each having a spectral band pass of 10 nm. We are presently investigating the possibility of using a single background suppression filter with a wider spectral band pass and sufficient transmission across a wider FOV. The increase in background noise should be at least partially offset by the increased speed of the fore-optics.

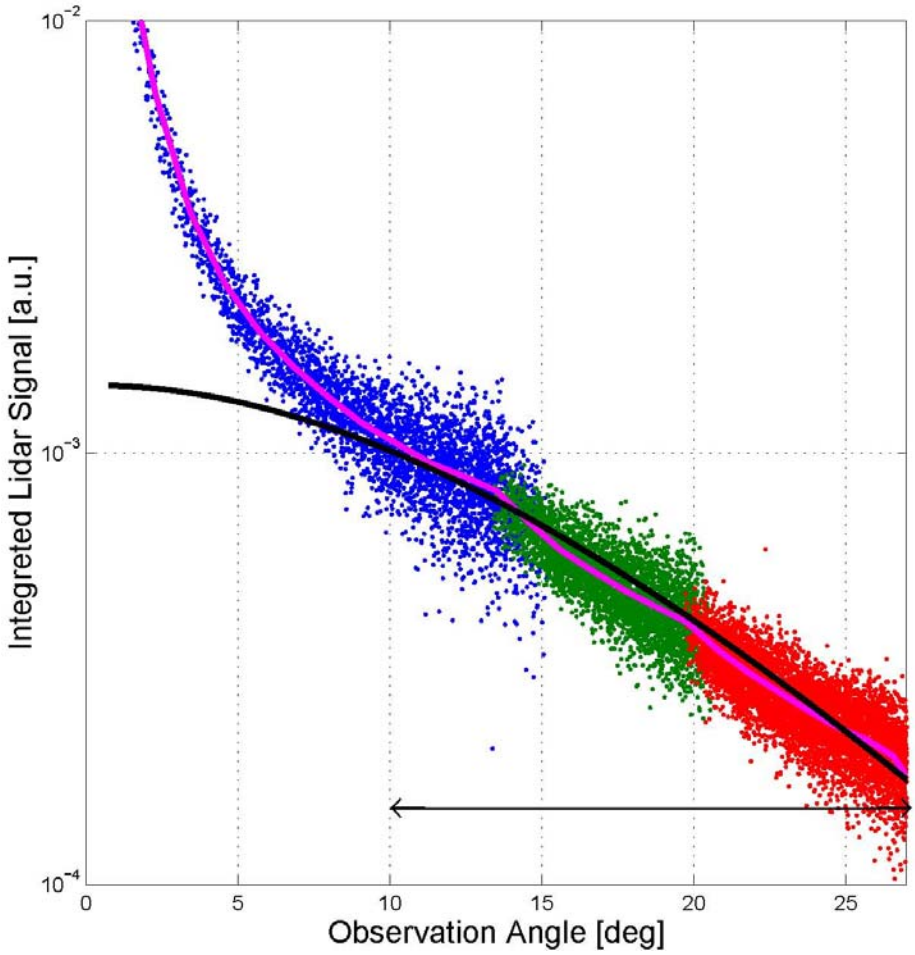

Figure 4. Time-integrated WAIL signal as a function of the viewing angle. The dots of 3 different colors correspond to WAIL measurements at 7:30 UTC through the 3 interference filters (cf. Figure 3). The colored line is a running mean through the WAIL data that was used in the regression. The solid black line is the best fit steady-state diffusion model (that assumes azimuthal symmetry). We have plotted here WAIL's (time-integrated) pixel values to show their dispersion due to natural variability of cloud structure as well as the instrumental noise. The latter noise component becomes more prominent toward the largest angels accepted by each filter.

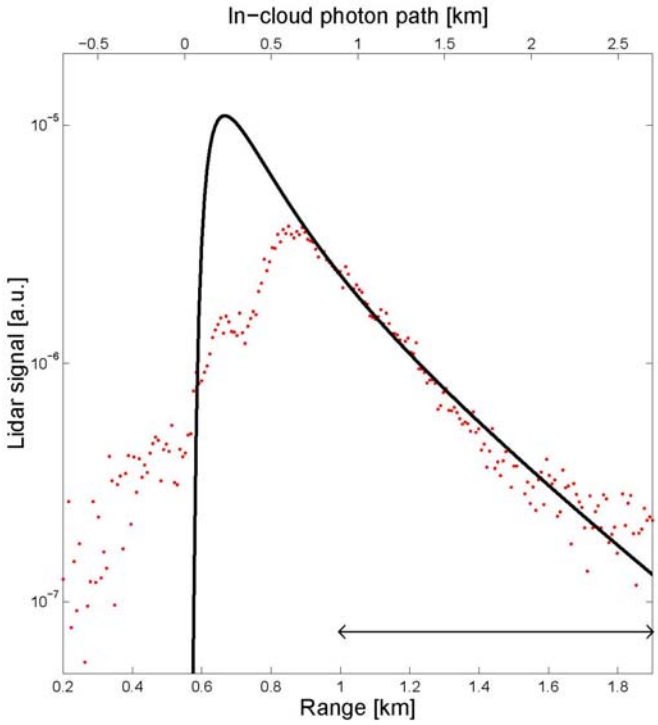

Figure 5. Time-resolved WAIL signal for pixels in a narrow annulus at viewing angle 26.6° as function of (1) the apparent range computed from a single-scattering assumption and (2) the actual in-cloud path accounting for multiple scattering. The dashed line is the best fit diffusion model using the same cloud parameters as in Figure 4. The nonlinear least-squares fitting procedure actually used the (useful ranges of the) spatial and temporal data in this and the previous figure simultaneously. The intervals highlighted with double-headed arrows along the horizontal axes indicate the ranges of angles and times deemed useful in the cloud parameter estimation. The diffusion-theoretical model used for the WAIL signal is not expected to work well for short paths and off-beam distances.

employed a non-linear fitting of the relevant diffusion theoretical prediction for WAIL signal (Polonsky and Davis 2005); see Figures 4 and 5. This provides us with the best cloud parameters in the least-squares sense. Our analysis shows that at 7:30 Universal Time Coordinates (UTC) H = 0.45 km and σ = 48 km^{-1} with uncertainties of 3 km^{-1} on σ and 0.09 km on H. At 8:00 UTC, we have H = 0.6 ± 0.2 km and σ = 50.5 ± 3 km^{-1}. The corresponding optical thickness estimates are τ = 21.6 ± 5.7 at 7:30 UTC and τ = 30.3 ± 11.8 at 8:00 UTC. How these estimations compare with the THOR estimation of the cloud top and ARM instruments' outputs is illustrated in Figures 6 and 7. The large uncertainties in the geometrical thickness and optical thickness, especially at 8:00 UTC, are directly traceable to the insufficient FOV in view of the low cloud ceiling (combined with relatively large cloud thickness). However, this problem has a straightforward optical solution and we anticipate improved accuracy in future deployments. The positive bias of the WAIL-derived liquid water path (LWP) is tractable to the standard (but ad hoc) assumption that cloud effective radius is 10 μm. It could well have been roughly 20% smaller and the results would then align.

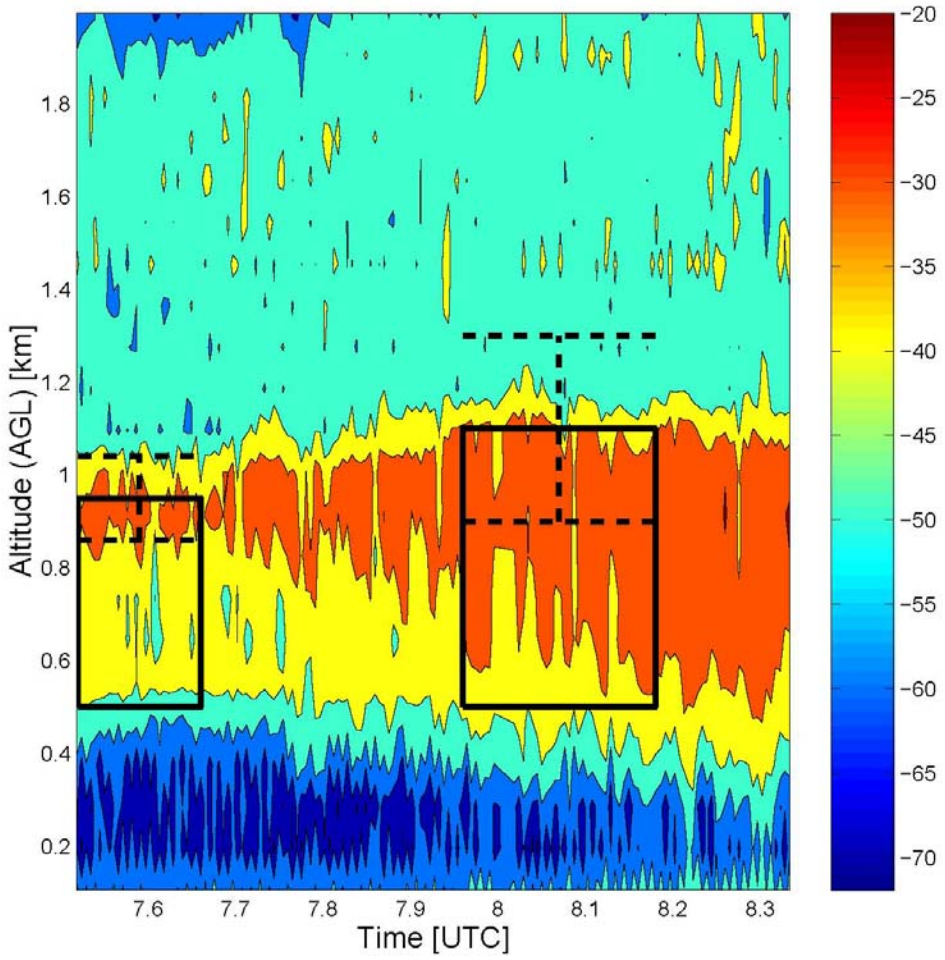

Figure 6. Cloud reflectivity (in dBZ) as a function of time and altitude above ground level retrieved from the millimeter wave cloud radar data. The layer with a strong reflectivity is situated between approximately 0.4 km and 1.1 km. The rectangles show the location of the cloud inferred from WAIL data (and the horizontally duration of the 3-filter collections) while the dashed lines depict uncertainties in the cloud top estimation.

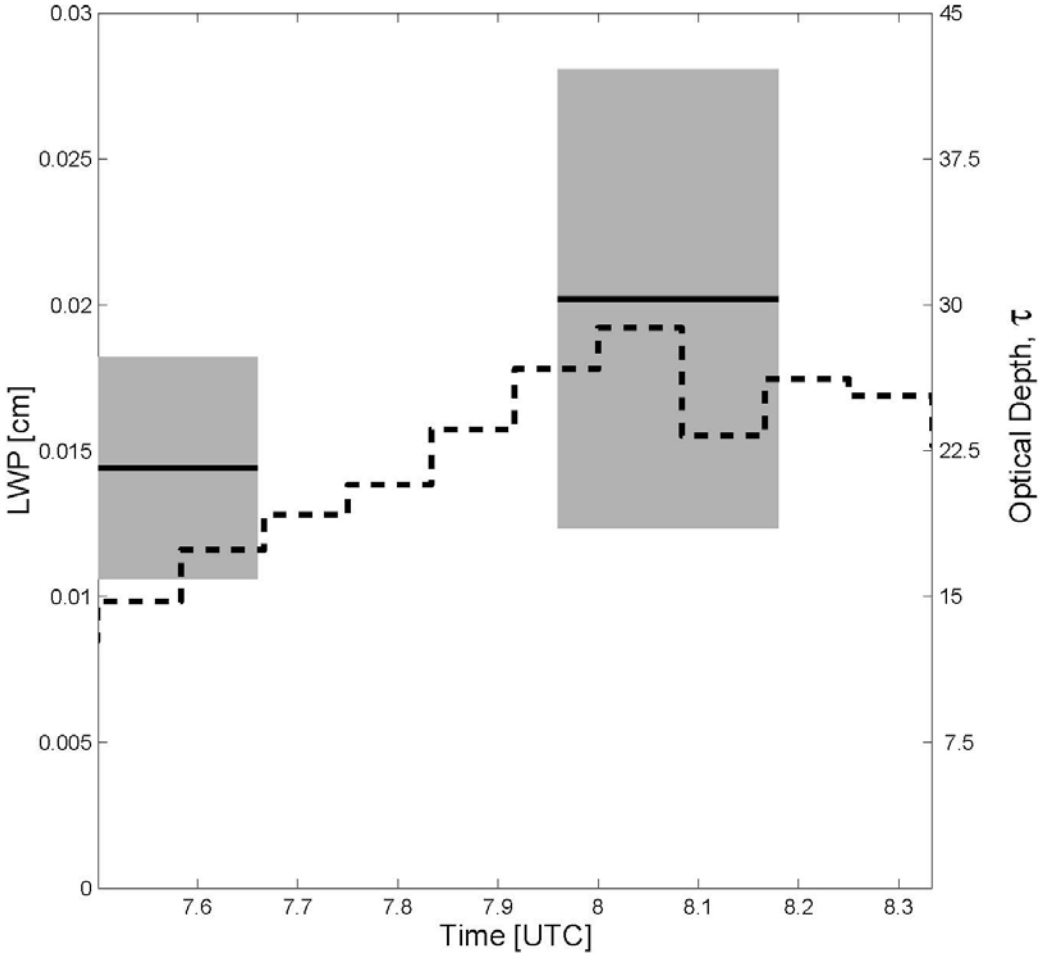

Figure 7. Liquid water path LWP (left axis) and cloud optical thickness (right axis) as a function of time. The estimation of the optical thickness from the microwave radiometer data (dashed line) may have as much as 20% error due to systematic uncertainty of the effective droplet radius (set here to 10 μm for simplicity). The horizontal solid lines show the optical thickness and associated LWP from the WAIL data while the grey patches show the estimated random error.

Concerning cloud observations with WAIL, we are currently refining our analytical diffusion-based model for the space-time signal to account for the frequently observed internal stratification of extinction; we will use a linear or power-law trend (either one requiring one extra parameter). Yet more realism can be achieved without leaving the framework of analytical diffusion models by incorporating one last parameterization for horizontal (turbulence-driven) variability; this is best done in the spirit of the independent-pixel approximation by mimicking the effective optical depth approach of Cahalan et al. (1994) or Barker's (1996) Gamma-Weighted Two-Stream Approximation.

Aerosol Profiling Capabilities

The full FOV of WAIL is focused onto an intensified/gated CCD array of 128-by-128 effective receivers; each of them operates independently and has a FOV of 7.4 mrad; note that this FOV is typical of devices targeting aerosol or plumes and that probe at medium range (a few km). Moreover, the WAIL signal (Figure 2) allows us to reconstruct time-resolved angular dependence of the atmospheric reflection. We can therefore consider the use of the WAIL signal to retrieve the properties of the aerosol layers situated between the WAIL receiver and probed cloud, or even under clear skies.

However, the aerosol probing has its own specific features. In particular, the probing has to be performed in the far zone which means that the detected signal either must not depend on the "overlap" function, or else this function has to be known (Kovalev and Eichinger 2004). Unfortunately, we had not measured this function for the cloud-driven deployment. Hence we have to estimate the time range when the overlap function can be considered unity. Because the WAIL receiver detects images, it corresponds a moment of time after which the position the maximum is stabilized and maintains its position on all following frames. To do so, we can use measurements performed on March 24. During this observation, the atmosphere was probed every 50 ns (7.5 m in range) starting from 700 ns time delay (113 m altitude) when the cloud base was detected at 450 m altitude. We can observe that the maximum location becomes stable after the 17^{th} frame which corresponds to a probing distance of 230 m. Let us invert the signal measured by the central pixel employing a version of the Klett algorithm (Klett 1981) assuming a constant lidar ratio. The results are shown in Figure 8 together with the results of the inversion of the MPL signal using the same algorithm. The disagreement at initial moments seems to be because of the overlap function is still not constant. Another possible reason is that the multiple-scattering contribution to the WAIL signal is much more significant than that of the MPL signal.

The MPL signal processing shows (Figure 8) that for the first 300 m the aerosol layer can be considered homogeneous. In this case the double scattering approximation predicts that the relative angular dependence of the reflected signal does not vary significantly with increasing probing distance. The angular dependence of the WAIL signal measured from the different altitudes depicted on Figure 9 is in agreement with this prediction. The dependence shown with the squares (■) is the signal detected from a range within the cloud layer and it is significantly different from other three dependencies measured from inside the aerosol layer at close range. In the case of homogeneous aerosol layer, this angular profile depends only on the phase function and, hence, may be used to retrieve selected parameters of the phase function, and, from those, the particle size characteristics (Bissonnette et al. 2005).

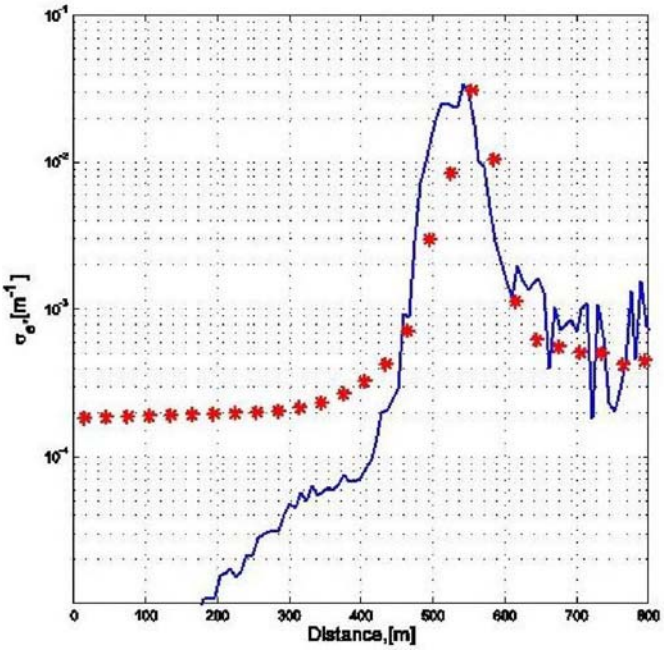

Figure 8. Extinction coefficient profile retrieved with a Klett-like algorithm assuming a monostatic configuration and a constant lidar ratio. We use as input either WAIL's (solid line) and MPL's (asterisks) returns.

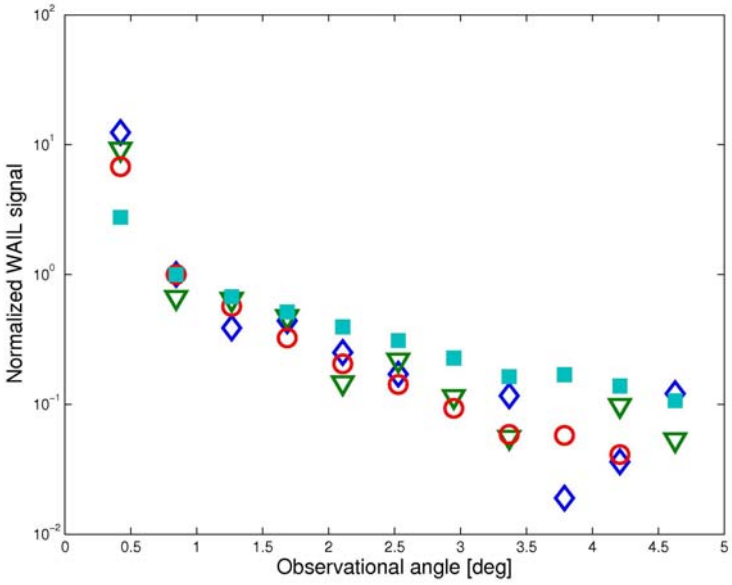

Figure 9. Angular dependence of the normalized WAIL signal measured for selected altitudes. Below the cloud, we have 180 m (◊), 293 m (▽), and 406 m (○). Notice that for the in-cloud range of 594 m (■) this angularly-resolved signal is significantly flatter than for the below-cloud ranges.

Making WAIL Smart and Autonomous

Currently, operation of WAIL requires a trained human supervisor whose responsibilities are (see Figure 10, human supervision):

a. controlling sensor functionality;

b. setting sensor parameters (time integration constants, number of pulses to collect) to provide a better signal-to-noise ratio and prevent receiver saturation;

c. validating correctness of the measured signal;

d. verifying measured signals to derive the selected parameters of the probed cloud.

Because of limited human supervisor availability to oversee sensor operation and, at the same time, to process measured signal, this scheme has a substantial drawback. If the operational parameters, which are set by the operator, are not adequate for a given atmospheric environment, the signal detected by the sensor may contain too little information to make possible successful operation of the signal processing algorithms (e.g., one for clouds and one for aerosols).

To eliminate this drawback one has to be able to forecast a trend of environmental change from the sensor's datastream and/or auxiliary sensors at the sensor platform. Then, if it is feasible, the sensor parameters can be adjusted adaptively. Since only quasi-plane-parallel stratus cloud morphology leads to analytical expressions for the WAIL signals, any scene which contains broken clouds requires an unacceptable amount of computer time for its simulation say by Monte-Carlo. Real-time simulations can therefore not be used. Moreover, an atmospheric model which includes horizontal inhomogeneities depends on too many parameters with extremely complicated inter-dependencies. This makes the use of look-up tables impractical. We plan to tackle this problem with a machine learning approach which will allow us to detect the presence of cloud boundaries by analyzing the measured signal, and, thus, to classify a given atmospheric environment into several predefined classes:
clear sky;

- continuous overcast cloud;
- transitional state between clear sky and overcast cloud;
- an isolated clouds with a finite aspect ratio.

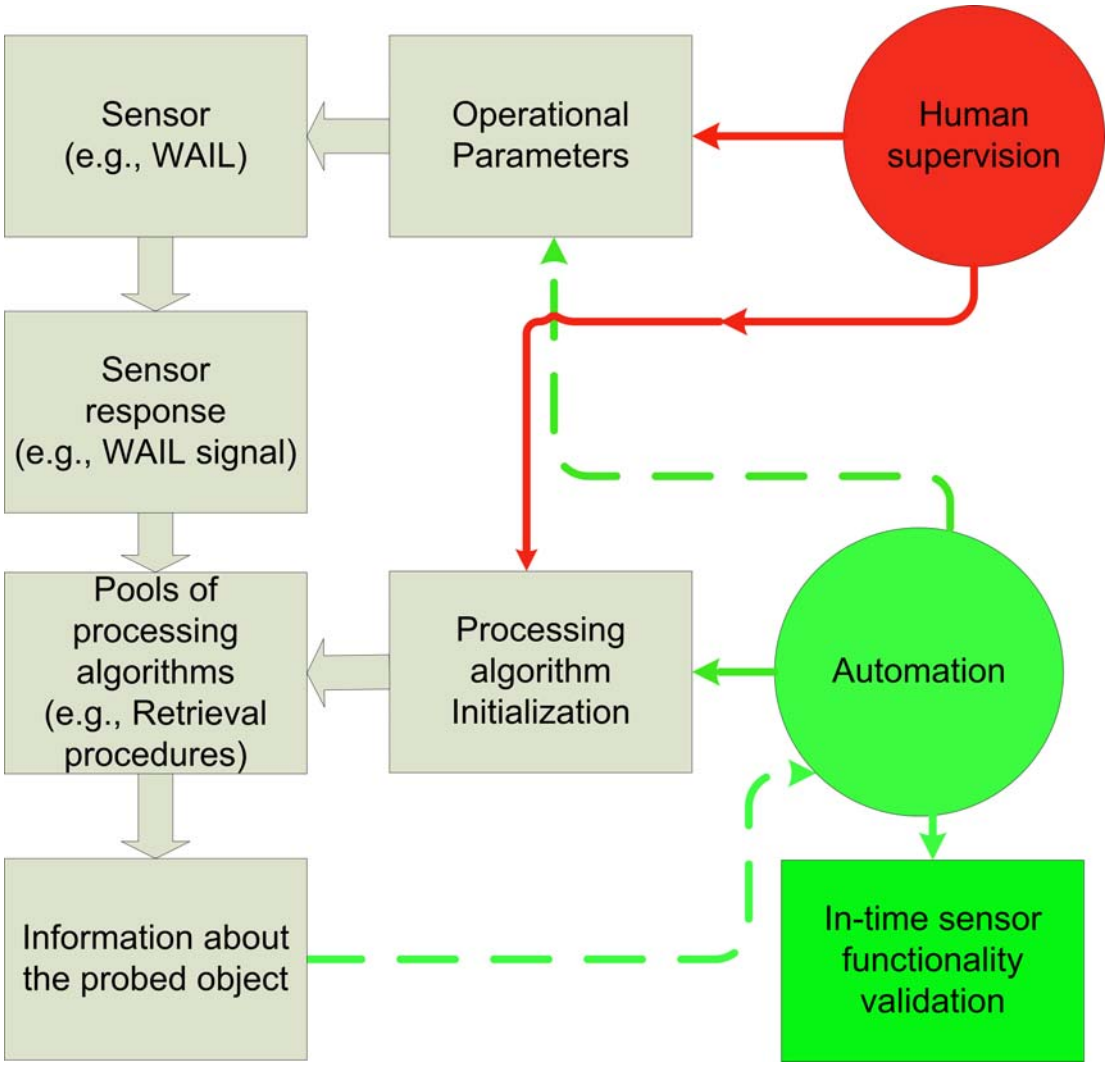

Figure 10. Proposed scheme for autonomous sensor operation: human supervision (red blocks) is replaced by code (green blocks) for instrument control, data acquisition and processing. Our approach is predicated on the use of a machine-learning framework, most likely based on genetic programming. During a period of "training" (by systematic comparison with collocated "master" instruments with known performance), this code "evolves" into a robust algorithm that will enable WAIL to operate adaptively under a wide range of atmospheric conditions. For instance, the integrated hardware-software sensor system will have to learn when to switch from cloud-probing to aerosol-probing modes which use radiative transfer models in opposite asymptotic regimes. We note that this paradigm may be applicable beyond WAIL to whole suites of environmental sensors.

This gives us the possibility to select an appropriate data analysis algorithm and, hence, to estimate the important parameters of the probed atmosphere. The history of parameter change allows us to predict the most probable direction of the change of the atmospheric structure (assuming persistence over the few minutes it takes to collect WAIL dataset). Optimal values of the sensor parameters are then adjusted as necessary to ensure successful monitoring.

The essential and most challenging part of this project is devising an approach to perform classification of the atmospheric conditions and finding parameterization schemes for them. In the case of overcast cloud this is not complicated, but for the case of broken clouds this is still an open question.

At the end of the project we expect to develop a sensor that

- will operate in daytime as well as nighttime (see Love et al. [2002]);
- is fully autonomous and self-checking;
- adaptively adjusts its operational parameters according to the current monitoring results;
- processes the sensor signal using the best algorithm from a pool of standard algorithms;
- estimates parameters of the atmospheric environment.

The major advantage is that the dataflow from such a sensor is free of errors due to operator fatigue or sensor operation parameters not being optimal. Additionally, the operational cost is minimal since expensive human operator supervision is not required.

Conclusions

With both LANL's ground-based WAIL and NASA's airborne THOR present, the validation campaign conducted at the SGP ACRF in March 2002 confirmed that off-beam lidar as a worthy concept to pursue in cloud remote sensing. The off-beam lidar retrievals of cloud characteristics from WAIL agreed well, within the established (and improvable) uncertainty, with independent observations of the cloud parameters by ARM instruments. Furthermore, we briefly describe straightforward ways of refining the diffusion-based model for the WAIL signal that will lead to more accurate and comprehensive characterizations of clouds in the solar spectrum, i.e., where it matters for climate.

Analysis of the earlier time bins demonstrated that the WAIL has the potential to be used to probe the aerosol layer beneath the cloud deck or, for that matter, under clear skies. However, the distance between the laser and receiver has to be decreased to the smallest possible value to approach to a mono static configuration as close as possible. The WAIL receiver has the advantage of providing the angular dependence of the atmospheric reflectance which can be likely used to retrieve some parameters of the phase function.

Finally, we discussed the roadmap we have drawn to make WAIL an autonomous, self-checking and adaptive instrument. Our strategy relies heavily on machine learning algorithms that improve by trial-and-error during a "training" period where WAIL's identification of sky conditions and subsequent retrievals are repeatedly compared with those obtained from collocated instruments.

Acknowledgments

We are thankful for the help of Mr. Larry Tellier (LANL/AIT-1) and of the SGP ACRF personnel during the "THOR/WAIL Validation Campaign" intensive operational period in March 2002. We are appreciative of the THOR team at NASA-Goddard for access to their excellent data for cloud-top height. We are grateful for the sustained financial support from the ARM Science Team and for funding received through LANL's LDRD/ER and -/PRD programs.

References

Barker, HW. 1996. "A parameterization for computing grid-averaged solar fluxes for inhomogeneous marine boundary layer clouds, Part 1: Methodology and homogeneous biases." *Journal of Atmospheric Science* 53:2289-2303.

Bissonnette, LR, G Roy, and N Roy. 2005. "Multiple-scattering-based lidar retrieval: method and results of cloud probings." *Applied Optics* 44:5565-5581.

Clothiaux, EE, MA Miller, BA Albrecht, TP Ackerman, J Verlinde, DM Babb, RM Peters, and WJ Syrett. 1995. "An evaluation of a 94-GHz radar for remote sensing of cloud properties." *Journal of Atmospheric and Oceanic Technology* 12:201-229.

Cahalan, RF, W Ridgway, WJ Wiscombe, TL Bell, and JB Snider. 1994. "The albedo of fractal stratocumulus clouds." *Journal of Atmospheric Science* 51:2434-2455.

Cahalan, RF, MJ McGill, J Kolasinski, T Várnai, and K Yetzer. 2005. "THOR, cloud Thickness from Offbeam lidar Returns." *Journal of Atmospheric and Oceanic Technology* 22:605-627.

Davis, A, DM Winker, A Marshak, JD Spinhirne, RF Cahalan, S Love, SH Melfi, and WJ Wiscombe. 1997. "Retrieval of physical and optical cloud thicknesses from space-borne and wide-angle lidar, in Advances in Atmospheric Remote Sensing with Lidar." A Ansmann, R Neuber, P Rairoux, and U Wadinger (Eds.), Springer-Verlag, Heidelberg (DGR), pp. 193-196.

Davis, AB, RF Cahalan, JD Spinhirne, MJ McGill, and SP Love. 1999. "Off-beam lidar: An emerging technique in cloud remote sensing based on radiative Green-function theory in the diffusion domain." *Physics and Chemistry of the Earth (B)* 24:177-185 (Erratum 757-765).

Davis, AB, DM Winker, and MA Vaughan. 2001. "First retrievals of dense cloud properties from off-beam/multiple-scattering lidar data collected in space, in Laser Remote Sensing of the Atmosphere: Selected Papers from the 20th International Conference on Laser Radar, Vichy (France), July 9-14, 2000." A Dabas and J Pelon (Eds.), École Polytechnique, Palaiseau (France), pp. 35-38.

Evans, KF, RP Lawson, P Zmarzly, and D O'Connor. 2003. "In situ cloud sensing with multiple scattering cloud lidar: Simulations and demonstration." *Journal of Atmospheric and Oceanic Technology* 20:1505-1522.

Love, SP, AB Davis, CA Rohde, L Tellier, and C Ho. 2002. "Active probing of cloud multiple scattering, optical depth, vertical thickness, and liquid water content using Wide-Angle Imaging Lidar, S.P.I.E." Proceedings, 4815: "Atmospheric Radiation Measurements and Applications in Climate," JA Shaw (Ed.), pp. 129-138.

Klett, JD. 1981. "Stable analytic inversion solution for processing lidar returns." *Applied Optics* 20:211-220.

Kovalev, VA, and WE Eichinger. 2004. Elastic Lidar: Theory, Practice, and Analysis Methods. John Wiley & Sons Inc., Hoboken (New Jersey).

Marshak, A, A Davis, WJ Wiscombe, and RF Cahalan. 1995. "Radiative smoothing in fractal clouds." *Journal of Geophysical Research* 100:26247-26261.

Polonsky, IN, and AB Davis. 2004. "Lateral photon transport in dense scattering and weakly-absorbing media of finite thickness: Asymptotic analysis of the Green functions." *Journal of the Optical Society of American A* 21:1018-1025.

Polonsky, IN, and AB Davis. 2005. Off-Beam Cloud Lidar: A New Diffusion Model and a Comparison with LITE Returns, Los Alamos National Laboratory Report, LA-14219, Los Alamos National Laboratory (New Mexico).

Polonsky, IN, SP Love, and AB Davis. 2005. "Wide-Angle Imaging Lidar (WAIL) deployment at the ARM Southern Great Plains site: Intercomparison of cloud property retrievals." *Journal of Atmospheric and Oceanic Technology* 22:628-248.

Winker, DM, RH Couch, and MP McCormick. 1996. "An overview of LITE: NASA's Lidar In-space Technology Experiment." In *Proceedings of the IEEE* 84:164-180.